

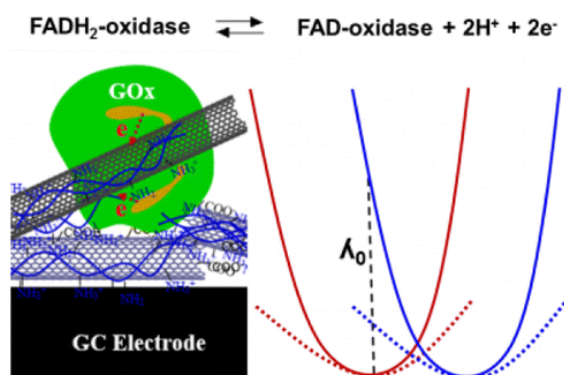
New evidence for a quasi-simultaneous proton-coupled two-electron transfer and direct wiring for glucose oxidase captured by the carbon nanotube-polymer matrix

By: Yiyng Liu, Tinatin D. Dolidze, Sameer Sanghal, Dimitri E. Khoshtariya, and [Jianjun Wei](#)

Y. Liu, T. D. Dolidze, S. Singhal, D. E. Khoshtariya, J. Wei, New evidence for a quasi-simultaneous proton-coupled two-electron transfer and direct wiring for glucose oxidase captured by the carbon nanotube-polymer matrix. *Journal of Physical Chemistry C*. 2015, 119 (27), 14900–14910. DOI: 10.1021/acs.jpcc.5b02796

This document is the Accepted Manuscript version of a Published Work that appeared in final form in *Journal of Physical Chemistry C*, copyright © 2015 American Chemical Society after peer review and technical editing by the publisher. To access the final edited and published work see <https://doi.org/10.1021/acs.jpcc.5b02796>.

Abstract:



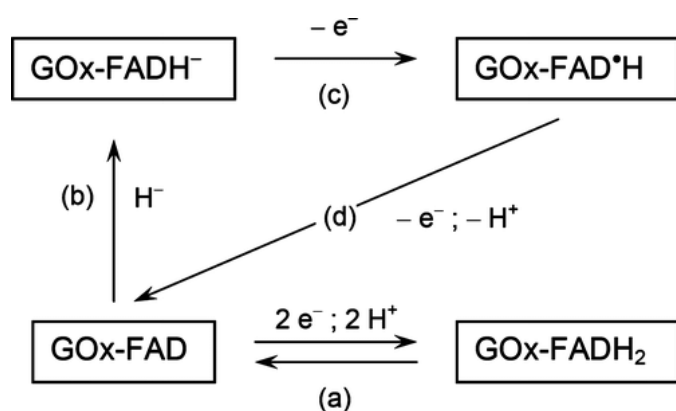
Systematic cyclic voltammetry (CV) studies of glucose oxidase (GOx) and its cofactor, flavine adenine dinucleotide (FAD), almost similarly captured by the matrix of single-walled carbon nanotube and polymer complex, in turn, deposited on GC electrodes have been performed. The comparative analysis of kinetic data obtained for the FAD and GOx specimens treated through the same Marcus theory-based algorithmic procedure strongly suggests that the GOx species, notwithstanding the deeply buried position of FAD, mechanistically behave virtually in the same manner as isolated FADs (the operationally capable, nearly intact structure of GOx was confirmed by the catalytic activity vs glucose), strongly suggesting that FADs inside GOx are directly wired to the GC electrode, presumably, via almost direct contact of nanotubes with both FADs residing inside each GOx biomolecule (as basically suggested by Guiseppi-Elie, A.; et al. *Nanotechnology* **2002**, 13, 559–564, and shortly supported by a number of valued researchers). Furthermore, the nonadiabatic, quasi-simultaneous two-proton-coupled two-electron transfer/exchange mechanism was concluded from further cross-analysis based on a generalized Marcus theory for the proton-coupled electron transfer (PCET), extra furnished by the first-time temperature-dependent CV studies and a subsequent Arrhenius treatment.

Keywords: Redox reactions | Charge transfer | Peptides and proteins | Electrodes | Carbon nanotubes

Article:

1 Introduction

Glucose oxidase—GOx (β -d-glucose: oxygen 1-oxidoreductase, EC 1.1.3.4) is an enzyme that catalyzes the oxidation of β -d-glucose to glucono- δ -lactone and the concomitant reduction of molecular oxygen to hydrogen peroxide.⁽¹⁻⁷⁾ Specifically, GOx from *Aspergillus niger* (the object of this particular study) is a dimeric flavoprotein consisting of two equal subunits with a molecular weight of ca. 80 kDa. Each subunit contains one flavine adenine dinucleotide (FAD) moiety. The enzyme is a glycoprotein containing eight potential sites for N-linked glycosylation, ca. 16% neutral and 2% amino sugars.⁽¹⁾ Two FAD moieties that are the catalytically active GOx cofactors are tightly but noncovalently incorporated within two active sites of the apoprotein situated ca. 15 Å below the protein “surface”.⁽⁸⁻¹⁰⁾ Along with its unique catalytic mechanism, GOx is also well-known for its bio(nano)technology applications.^(3, 11) Therefore, GOx enzymes from different biological sources, along with a variety of their supramolecular assemblies, fall within the scope of most intriguing and extensively studied biological or biomimetic objects. In particular, GOx entities immobilized on macroscopic carrier-deposited carbon nanotubes (CNT) attracted much attention since they demonstrated superior electron exchange currents compared to other interfacial configurations.⁽¹²⁻¹⁵⁾ One group of researchers interpreted this fact as an indication of deep penetration of the nanotubes’ tops that lean out of the average “facade” and may enter into the GOx interior to provide almost direct contact with FADs residing therein (“direct wiring” for electronic tunneling).⁽¹²⁻¹⁵⁾ However, recently, Gorski et al.,⁽¹⁶⁾ based on their distinct experimental results, doubted the intactness of GOx entities brought in contact with carbon nanotubes, hence questioning this attractive general conjecture. In this paper, along with the mechanistic aspects of electron exchange within the GC/CNT-polymer/GOx composite systems, we will directly address the issue of the GOx integrity and the role of CNT components as “personal nanoelectrodes” within these assemblies.



Scheme 1. Fully Oxidized Quinone (GOx-FAD), Fully Reduced Hydroquinone (GOx-FADH₂), Partially Reduced (GOx-FADH⁻), and the So-Called Semiquinone (GOx-FAD[•]H) States of FAD

In general, FAD, like other quinones, may undergo concerted two-electron (Scheme 1a, b) or sequential one-electron (c, d) redox transformations coupled to proton(s) translocation(s).⁽¹⁻⁷⁾ According to contemporary views,⁽¹⁻⁷⁾ in the course of a GOx catalytic cycle FAD accepts hydride ion (H⁻) from glucose to produce a lactone in a reductive step (b), and in a subsequent

oxidative step (c) donates one electron to form a semiquinone and free radical intermediate of oxygen.^(1, 2, 5-7) Step (d) generates H₂O₂ and regenerates the enzyme. The situation is different and much more ambiguous in the case of FAD redox processes at electrodes, with or without the GOx globule serving as an environment (implying the absence of any catalytic transformation of organic substrates). These interfacial, actually man-made, processes exhibit the CV response with distinct single anodic and single cathodic Faraday peaks reasonably attributable to the chemically reversible concerted two-electron pattern (Scheme 1a).^(12, 15, 17-22) However, although only one couple of peaks can be observed, the mechanism hardly can be the “true” simultaneous two-electron transfer event implying equal formal redox potentials for each single ET since the reactant’s two successively appearing states are essentially different.

According to the previous analyses,^(17-21, 23, 24) in general terms, formally, two single-electron transfer steps can be considered with two respective formal equilibrium potentials, E_1^0 and E_2^0 . When $\Delta E^0 = E_2^0 - E_1^0 < -100$ mV, two couples of individual redox peaks appear corresponding to “independent” single-electron transfers. When ΔE^0 is between 0 and -100 mV, the individual waves are merged into a broad wave whose peak potentials (E_p) are independent of scan rate. When $\Delta E^0 = 0$ (the case already mentioned above) a single-peak current intermediate between those of a single-step reaction is found, and when $\Delta E^0 > 180$ mV (i.e., the second step is easier than the first), a single couple of peaks appear with a single effective equilibrium potential, E_{eff}^0 . In the latter case the two-electron transfer is considered as apparently (or quasi-) simultaneous.^(17-21, 23, 24) This reasoning, except some numerical details for the peak shapes specifically determined by the reactants’ operational regime (the freely diffusing versus surface-confined modes), clearly, is common and naturally rests on fundamentals of the contemporary charge-transfer theory (vide infra).

In a recent paper by Bond et al.,⁽²⁰⁾ the possible mechanisms for GOx immobilized on various carbon-based electrodes (and implied to be “operationally capable”) were considered including consecutive one-electron transfer versus concerted transfer, the latter including true simultaneous and quasi-simultaneous two-electron transfers, respectively. Application of advanced multilevel Fourier transform ac voltammetry and respective simulations, based on a range of models, allowed only for a general conclusion in favor of quasi-simultaneous two-electron transfer and the extra specific mechanistic complexity, seemingly due to the involvement of a diffusional motion of reactive protons and the accompanying conformational transformation of the FAD cofactor itself, suggested the latter as resulting in the so-called “gated” mechanism for the ET process.⁽²⁰⁾ Further efforts with the involvement of the Marcus model yielded a rather low value for the reorganization energy (≤ 0.3 eV, vide infra) and a broad spectrum of floating values for the effective rate constant, spanning over 5–3000 s⁻¹.⁽²⁰⁾

Obviously, further in-depth experimental studies and theory-based analyses were required for a better comprehension of the GOx and FAD multifaceted redox mechanisms using additional experimental approaches such as, e.g., temperature-assisted kinetic cyclic voltammetry (CV) studies, allowing independent determination of the additional important physical parameter—the enthalpy of activation—thus providing a complementary way for the verification of the reorganization energy; hence, our work offers a new prospect for a thorough testing of the ET pattern (vide infra). In the present paper, we report on fundamental studies of electron transfer of GOx that is immobilized into a single-walled carbon nanotube–poly(ethylenimine) (SWCNT–

PEI) matrix. For a comparative purpose, the redox performance of isolated FAD immobilized on the same type of electrodes in a similar manner has been explored as well. Along with the first-time temperature dependence studies for the effective two-electron transfer rate constant, we demonstrate more systematic application of the extended Marcus theory (that goes beyond the medium's linear response prototype, see below) to voltammetric data and the rigorous data cross-testing. Moreover, the electrocatalytic effect on glucose confirms the intact structure of the closely entrapped (CNT-wired) GOx.

2 Experimental Section

Materials

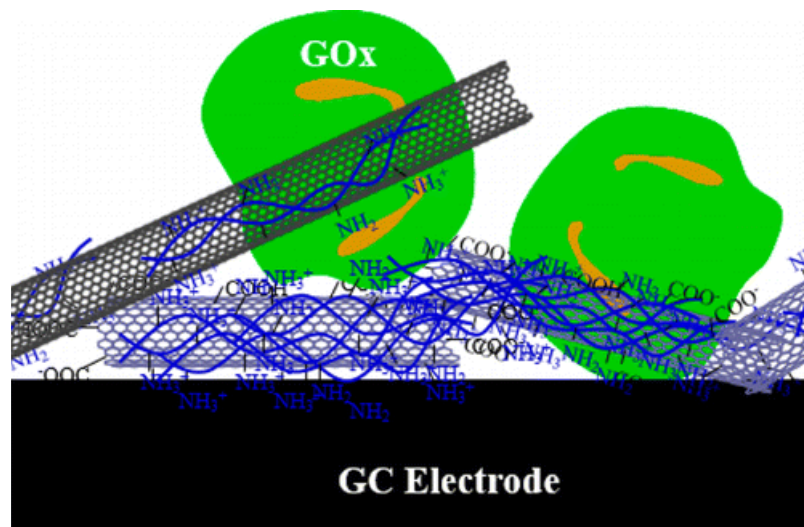
Glucose oxidase (EC 1.1.3.4, type VII-S), *N*-hydroxysuccinimide (NHS), *N*-(3-(dimethylamino)propyl)-*N'*-ethylcarbodiimide hydrochloride (EDC), poly(ethylenimine) solution (MW 25 000, 50% w/v in water) were purchased from Sigma/Aldrich and used without further purification. Carboxylate functionalized single-walled carbon nanotube (SWCNT-COOH, 2.73% -COOH content, 95 wt % purity, OD 1–2 nm, 5–10 μ m length, EC > 100 s/cm) were purchased from Cheap Tubes, Inc. Glucose stock solutions were prepared in variable concentrations from 5 mM to 1 M in 20 mM/0.1 mM KCl with phosphate buffer solution (PBS) of variable pH, respectively. Stock solutions were stored overnight to allow equilibration before the usage. All other chemicals employed were of analytical grade and used without further purification. Deionized water (18.2 M Ω) was obtained through Micropore filter system.

Preparation of GOx Electrodes

Glassy carbon (GC) electrodes (3 mm in diameter) were polished with 1.0, 0.3, and 0.05 μ m alumina slurry sequentially and then ultrasonically washed in water and ethanol for a few minutes, respectively. The cleaned GC electrodes were dried with a high-purity nitrogen stream.

The GOx/PEI/CNT assembled GC electrode was fabricated using a layer-by-layer process. Briefly, the COOH functionalized CNT was dispersed in *N,N*-dimethylformamide (DMF) solvent with a concentration of 1 mg/mL and sonicated for 30 min at 60 W using a strong ultrasonic processor (Sonicator, S-400, Misonix, Inc.) with a microprobe system. The subsequent analysis of the treated SWCNTs by strong ultrasonification indicated that the average in situ length was a few hundreds of nanometers or less, that is, comparable to the dimensions of a GOx macromolecule (see discussion below and the Supporting Information). An aliquot of the CNT solution was dropped onto a polished GC electrode surface (3 mm diameter; CHI Instruments), and the coating was allowed to dry completely in a cleaned incubator at 45 $^{\circ}$ C. We performed different CNT loading volumes ranging within 0.2–2.5 μ L and found 0.6 μ L of the SWCNT-COOH solution was the best for reproducibility in electrochemical responses (cyclic voltammetry and catalytic oxidation of glucose, etc.) and the collection of direct electron transfer data of GOx. Hence, the results of this study were obtained using a fixed loading volume (0.6 μ L) of CNT solution if not otherwise specified. The CNT-coated GC electrode was then washed carefully with DI water. Prior to soaking the CNT-coated electrode in 1 mg/mL poly(ethylenimine) (PEI) to self-assemble the positive charged polymer to the electrode, the electrode was first dipped in a 1 M NaOH solution for 5 min to introduce more negative charges

and rinsed with DI water. After 10 min of incubation in PEI solution, the CNT/PEI-coated electrode was rinsed with DI water and then incubated in a freshly prepared 50 mM HEPES (pH 7.1) buffer solution containing 1 mg/mL GOx and 0.5 mM EDC/NHS for cross-linking the protein GOx to the PEI/CNT-coated electrode. The GOx was immobilized to the CNT/PEI-coated electrode after 2 h incubation and then washed using the HEPES buffer solution to get rid of loosely attached GOx. Scheme 2 illustrates a hypothetical arrangement of the GOx/PEI/CNT electrode schematically depicting the direct contact (wiring) of the GOx to CNTs.



Scheme 2. Sketch of the SWCNT/PEI/GOx Matrix at Glassy Carbon (GC) Electrode^a

Scheme a. A hypothetical arrangement of the matrix to illustrate the possible configuration of GOx molecules that are directly wired to the GC electrode via CNTs' contact with FADs inside GOx (see Results and Discussion for more details).

In order to ensure the protein immobilization, we used a high ionic strength supporting solution (20 mM PBS plus 0.1 M KCl) for all the electrochemical experiments, and each electrode was incubated in the solution for 10 min to stabilize the electrode. The weakly bonded proteins were supposed to be dissociated from the electrode under these conditions.⁽²⁵⁾ The electrochemical response was checked after 10 days, and the peak current of GOx redox reaction maintained a level of 80% or more of that in the first day after preparation, suggesting a stable immobilization of the enzyme in the CNT/PEI matrix.

Cyclic Voltammetry

Cyclic voltammetry (CV) was performed using a CH Instrumental Electrochemical Analyzer 412A controlled by a PC computer running CHI software. The three-electrode cell was composed of a platinum wire counter electrode, an Ag/AgCl (3 M KCl) reference electrode, and the CNT/PEI/GOx-modified GC electrode as a working electrode. The voltammetric measurements were performed in 20 mM phosphate buffer solutions containing 0.1 M KCl. On the one hand, usage of supporting electrolytes with sufficiently high ionic strength warrants low-solution iR drop. On the other hand, each CNT/PEI/GOx-modified GC electrode was incubated in the supporting solution for 10 min before data collection to allow the dissociation of the

loosely absorbed enzyme from the CNT/PEI matrix. To study the pH effect, the voltammetry was carried out using the pretreated enzyme electrode in working solutions at different pH values ranging from 4.6 to 8.0 (PBS solutions containing 0.1 M KCl). The temperature of the electrochemical cell was controlled by a circulating water bath (VWA-3500A), and all CVs were collected in PH 7 supporting solutions.

CV measurements of GOx were performed at several temperatures, from 0 to 45 °C (0, 5, 15, 25, 35, 45 °C). For each temperature, the measurements were repeated three times using freshly prepared electrodes. The voltammograms were collected with the scan rates increasing from 10 mV/s to 10 V/s at the SWNT/PEI/GOx carbon glassy electrodes. Normally, the peak separation of an experimental voltammogram arises from a kinetic factor and an uncompensated solution resistance, R_u . We removed the possible effects of R_u by applying a “post-measurement” correction in the data analysis as reported earlier.⁽²⁶⁾

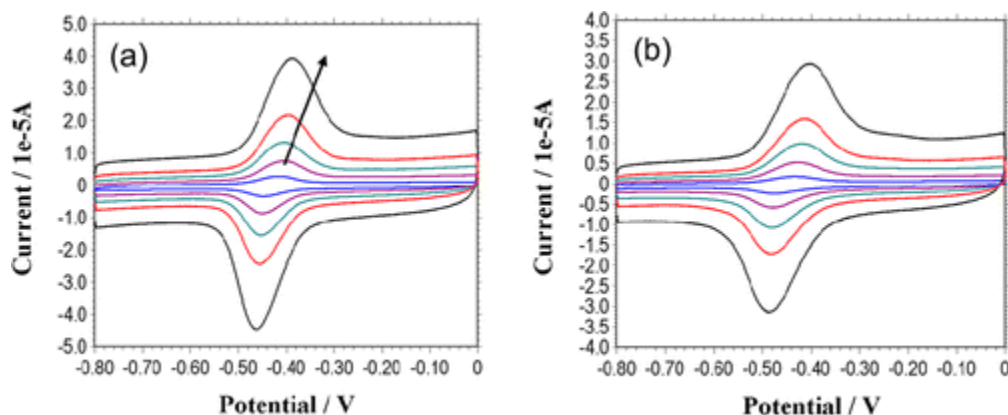


Figure 1. Representative CVs of GOx (a) and FAD (b), entrapped into the SWCNT/PEI matrix. CV scan rates are 10, 30, 60, 100, and 200 mV/s at 25 ± 0.5 °C (peak current uprising as the array shows). All temperature-dependent CVs at scan rates up to 3000 mV/s are included in Supporting Information.

3 Results and Discussion

The Primarily Analysis of CV Data

The above-described composite nanostructured electrodes, with the GOx entities entrapped therein, display very well-pronounced and highly reproducible voltammetric (Faradaic) response. Figure 1a shows representative cyclic voltammograms (CVs) at variable potential scan rates. First of all, we mention that the Faraday peak current of experimental CV curves (Figure 1) exhibits a biphasic pattern as a function of the potential scan rate changing from the linear dependence (the immobilized redox couple) to the square root one, which are typical for the “purely” surface-confined and “mixed” diffusion-limited electrode processes, respectively,^(23, 24) see Figure 2 and the Supporting Information. Seemingly, the term mixed indicates ET exchanges with the FAD moieties kept inside surface-confined GOx molecules, in which the translocation of proton(s) becomes diffusion-limited at higher scan rates.⁽²¹⁾ The “naked” FADs directly adsorbed at SWNT/PEI electrodes may suffer similar kinetic constrains caused by impact of the environmental overcrowding. In addition, the data for the CV peak widths (fwhh), 74/–8 mV at

10 mV/s, are narrower than that expected for one-electron transfer, and the pH dependence of the formal redox potential is 52 mV/pH (over the range of pH 4.5–8.0, see the Supporting Information). These results, in general, are consistent with a quasi-reversible, two-proton-coupled two-electron exchange process^(12, 15, 17-22) (however, see further discussion below). Isolated FAD under otherwise the same conditions displayed very similar performance (see Figure 1a and b, and Supporting Information Table S3). The wider fwhh for FAD (94–102 mV at scan rate 10 mV/s) seems to be consistent with a peak extra broadening due to the system's inhomogeneity, viz., broader spatial distribution of redox-active FAD species compared to redox-active GOx species (because of the proposed very specific configuration for redox-active GOx species, see Scheme 2 and the discussion below), rather than the manifestation of a quasi-reversible one-electron transfer process.

Data Fitting through the Marcus Model

The adequate mechanistic understanding of ET processes, in general, requires accurate determination of key parameters, the standard rate constant, k^0 , reorganization Gibbs free energy, λ_0 , and the electronic coupling, V_{AB} , self-consistently defined within the extended, yet linearly “responsive”, Marcus theory.⁽²⁷⁻³²⁾ In the case of proton-coupled electron transfer (PCET), the latter parameter is modulated by the wave functions of reacting proton(s), vide infra.⁽³²⁻³⁵⁾ The most straightforward and advanced method for the purpose of determination of k^0 and λ_0 currently is the CV data-processing algorithm based on the extended Marcus theory, developed by Weber and Creager^(36, 37) and Murray et al.,⁽³⁸⁾ see also ref 39. In a general form, the reduction and oxidation rate constants can be expressed by the equations

$$k_{\text{red}}(\xi) = A \int \exp\left[-\frac{[(\varepsilon_F - \varepsilon) + e\xi + \lambda_0]^2}{4\lambda_0 RT}\right] [f(\varepsilon)] \frac{d\varepsilon}{RT} \quad (1)$$

$$k_{\text{ox}}(\xi) = A \int \exp\left[-\frac{[(\varepsilon_F - \varepsilon) - e\xi + \lambda_0]^2}{4\lambda_0 RT}\right] [1 - f(\varepsilon)] \frac{d\varepsilon}{RT} \quad (2)$$

In eqs 1 and 2, λ_0 is the overall (resulting) reorganization energy of the system (vide infra), ξ is the overpotential (equal to the applied potential relative to the formal potential of the redox specie), ε_F is the Fermi energy (equal to the applied potential), $f(\varepsilon)$ is the Fermi function, R is the gas constant, T is absolute temperature, and A is a pre-exponential factor whose form is specific for the intrinsic ET mechanism (to be specified below). The term ε is an integration variable that corresponds to the energy of the electronic levels in the electrode.

Application of this algorithm (actually, the data-fitting procedure) to peak separation data (Figure 1) unequivocally demonstrated an anomalous pattern which obviously does not originate from trivial reasons such as the poor Faradaic-to-background current ratio or the large (even sizable) uncompensated Ohmic drop (IR_u). Actually, neither the whole sequence of experimental points, nor its low- or high-overvoltage regions, could be satisfactorily fitted by theoretical (classically shaped) “trumpet” curves, see Figure 3a. Importantly, analogous processing of CV data for isolated FAD displayed a very similar pattern, see Figure 3b, yielding similar floating ranges for respective kinetic and reorganization parameters (Supporting Information, Table S4). This anomaly obviously is of the same nature as the one encountered in the previous work by

Bond et al.,⁽²⁰⁾ however manifested in somewhat different way as dissimilar data-processing algorithms were applied. Because theoretical trumpet curves are generated on the basis of “classical” Marcus theory implying quadratic shapes for resulting reactant/product energy wells (implying the medium’s linear response) which determine free energy relationships for ET, it seems natural to ascribe the anomalous shapes of experimental trumpet plots to the deviations from the classical harmonic shapes for actual free energy wells.

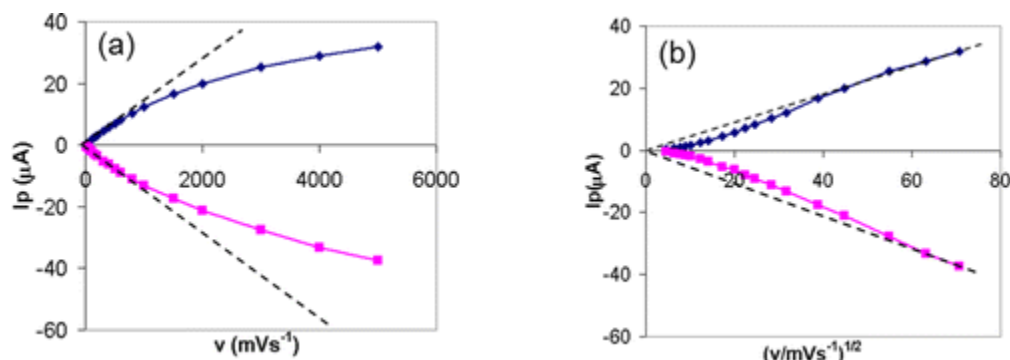


Figure 2. Panels (a) and (b) display graphs presenting the dependence of peak current on the voltage scan rate and the square root of the voltage scan rate, respectively. Data obtained from a SWCNT/PEI/GOx electrode at pH 7.0; blue is anode, and purple is cathode.

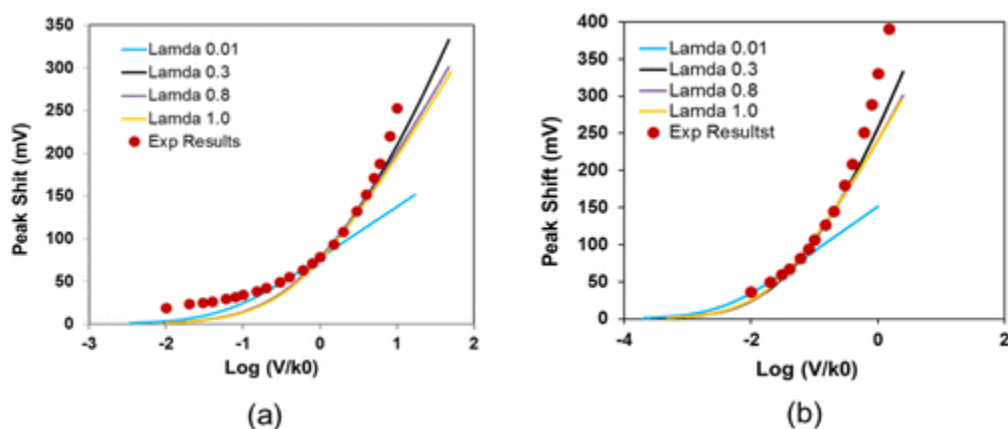


Figure 3. Representative CV data for peak potential shifts (red circles) as a function of the scan rate reduced to the rate constant (pH 7, 25 °C) for a GOx electrode (a) and FAD only electrode (b) under the same experimental conditions. The solid curves with different colors are fit to the Marcus model with λ_0 of 0.01, 0.3, 0.8, and 1.0 eV, as indicated in figure captions.

The main result of fitting of the obtained data according to classical Marcus theory is that by entering the experimental values representing different overvoltages (probed within different windows of potential scan rates), for a given ET process with different theoretical curves fitted to different ranges of experimental points, one may obtain virtually unlimited number of different pairs of parameters, k^0 and λ_0 (e.g., $\lambda_{o(1)} = 0.01$ eV and $k^0_{(1)} = 1.3$ s⁻¹, and $\lambda_{o(2)} = 0.8$ eV and $k^0_{(2)} = 4.1$ s⁻¹, 25 °C). This result is an obvious deviation from the “standard” case, which, in light of the currently developing landmark views,⁽⁴⁰⁻⁴²⁾ can be logically ascribed to the breakdown of the medium’s liner response paradigm (since eqs 1 and 2 directly imply the quadratic shape for Gibbs energy wells). The general description of deviations from the linear

response model specifically for *biomolecular or bio-mimicking ET processes* most extensively (yet not exhaustively) has been deliberated by Wolynes et al.,^(40, 41) Zewail et al.,⁽⁴²⁾ and Matyushov et al.^(43, 44) According to Matyushov,^(43, 44) for ET events occurring in sluggish, glass-forming environments, including biomolecular systems, the breakdown of the medium's linear response pattern is a general occurrence closely linked to the breakdown of another conventional paradigm entailing the system's ergodicity. Some experimental (electrochemical) manifestations attributable to these kind of anomalies for biomolecular and biomimetic ET were reported recently.^(45, 46) In brief, for ET processes, occurrence at nearly zero driving force (in electrochemistry, around zero overvoltage) conditions (that correspond to moderate ET rates), the comprehensive theoretical consideration predicts essential lowering of the Gibbs energy barrier (actually, of the effective reorganization free energy) owing to "freezing out" of the slowest conformational (relaxational) reorganizable degrees of freedom (modes).^(43, 44) At higher overvoltages, generally speaking, ET rate tends to increase due to the increase of the (negative) energy gap; however, due to the system's nonergodicity (if the case), also a value of the effective reorganization free energy starts to dramatically increase, thanks to the progressive inclusion of additional, increasingly faster conformational (relaxational) modes.^(43, 44) This would lead to the breakdown of the constancy for the standard value of the rate constant, k^0 , when probed at higher overvoltages, turning the physical meaning of the standard fitting procedure questionable. So, typically, for glass-forming systems, the concept of "standard rate constant" would increasingly lose its unambiguous physical meaning, when going from the lower to higher scan rates (overvoltages). Meanwhile, importantly, the term of "reorganization Gibbs energy", λ_0 , attains the dual, yet clear physical meaning, see refs 43, 44.

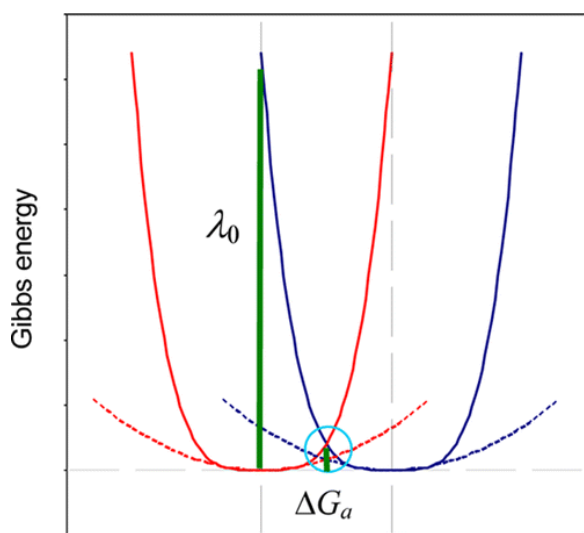


Figure 4. Schematic illustration of shapes for the hypothetical fourth-order (quartic) reactive Gibbs energy wells (solid curves) for electron exchange at zero overvoltage (zero energy gap). The dashed curves illustrate quadratic (harmonic) approximation for the bottoms of the quartic wells. Vertical green bars are to illustrate the reorganization (λ_0) and activation (ΔG_a^*) motifs. One can see that the difference for the heights of the curve intercept points (matching values for ΔG_a^*) is of a factor of 2.5, while the difference for the heights of vertical transitions (matching values for λ_0) is of the factor of 10.⁽⁴⁵⁾ Note, the real curves are supposed to be of the hybrid nature; however, the conjecturing is valid throughout; see text for more details.

In this context, one may also consider the simplified approximation to an above-mentioned complicated pattern by using the operational quartic (fourth-order) energy wells,^(47, 48) Figure 4 (see also ref 45). One can estimate that assuming the same values of activation Gibbs energies for the extreme cases of pure quartic and pure quadratic wells, the respective value of λ_0 for the quartic case should be four times that for the harmonic (quadratic) one.⁽⁴⁵⁾ Furthermore, a formalistic application of the conventional (quadratic) algorithm to the actual quartic situation results in $k^0_{\text{(eff)}}$ that attains its more or less physical meaning when determined at lower scan rates (probing lower values of overvoltages, where $\xi \rightarrow 0$), while at higher overvoltages, the values of $k^0_{\text{(eff)}}$ would increase, and, although remaining of the same order of magnitude, would become hardly interpretable. Furthermore, it has been discussed earlier^(20, 21) that the accompanying inner-sphere conformational transformation of FAD^(21, 58) may have an impact on the ET rate through some essential contribution to the activation motif, related, e.g., to the “gating” mechanism, conjectured before.⁽²⁰⁾ We argue that such a contribution may emerge as a part of the entire inseparable concerted process rather than show up as a separated, hardly interpretable (specifically, in terms of the CV signal performance) conformationally gating stage. Our expectation was that the first-time temperature-aided CV measurements (Arrhenius analysis) for the proton-coupled two-electron electrode process involving GOx could shed light onto the respective mechanistic interpretation (see discussion in the respective subsection below).

The Basic Mechanistic Analysis

In order to continue further the adequate mechanistic analysis, a thorough comparison of results obtained through the application of two independent experimental approaches (implying the peak separation versus scan rate and Arrhenius studies), one requires choosing the adequate operational kinetic equation of two basic ones, offered by the generalized charge-transfer theory. In the framework of a conventional version of this theory (yet resting on the medium’s linear response approximation), any of eqs 1 or 2, depending on the type of the intrinsic charge-transfer mechanism (showing up through the prefactor A), may cast in either eq 3 or eq 4^(29-32, 49-54)

$$k^0_{\text{ET(NA)}} = \frac{V_{\text{AB}}^2 \rho_{\text{m}}}{\hbar} \sqrt{\frac{\pi^3 RT}{\lambda_0}} \exp\left(-\frac{\Delta G_{\text{a}}^*}{RT}\right) \quad (3)$$

$$k^0_{\text{ET(DC)}} = \nu_{\text{eff}} \sqrt{\frac{\lambda_0}{\pi^3 RT}} \exp\left(-\frac{\Delta G_{\text{a}}^*}{RT}\right) \quad (4)$$

where k^0 is the standard electron-transfer rate constant, defined as a rate constant under zero overpotential (zero Gibbs energy gap) condition, at which the process is controlled by electron exchange at the electrode’s Fermi level. Furthermore, V_{AB} is the resonance energy for electronic coupling between the electron donor and acceptor states (alternatively, this symbol may imply the overall resonance energy in the case of PCET processes), ρ_{m} is the density of electronic states within the electrode (acting as a reactant) around the Fermi level, ν_{eff} is the effective frequency of the medium’s fluctuations coupled to ET (or PCET), and ΔG_{a}^* is the activation Gibbs free energy here defined as (vide infra)^(29-32, 49-54)

$$\Delta G_s^* = \frac{\lambda_0}{4} - V_{AB} \quad (5)$$

Although, in a number of remarkable cases, performance of both the nonadiabatic (eq 3) and dynamically controlled (apparently adiabatic, eq 4) mechanisms and even the smooth changeover between them for biomolecular interfacial redox processes has been convincingly demonstrated,⁽⁴⁹⁻⁵⁴⁾ one may consider cases in which distinguishing between two mechanisms could be difficult. This supposition is especially true for cases of ET processes that are complicated by coupled (essentially integrated) events such as stoichiometric proton transfer(s), local and/or extended conformational transformations, etc.^(35, 45, 46, 55) For instance, in the case of PCET which is proposed for the concerted process under consideration (Scheme 1, process a) if the nonadiabatic mechanism (eq 3) is operative, the pre-exponential term of relevant kinetic equation should contain combined tunneling probabilities of two electrons and two protons. In this case, the symbol V_{AB} represents the overall resonance coupling energy, which can be written as $V_{AB} = H_{AB} \times L_{AB}$, where H_{AB} is the resonance energy for electronic coupling and L_{AB} is the overlap integral of the proton(s) vibration wave functions; the parameter H_{AB} varies with the electron transfer distance, R_e , according to $H_{AB} = H_{AB}^0 \exp[-\beta/2(R_e - R_0)]$ in which H_{AB}^0 is the value of H_{AB} at the closest electron donor–acceptor separation, R_0 , and β is the empirical decay parameter for it. If the involvement of two electrons, for some reasons cannot warrant the overall nonadiabaticity (that is, the process is adiabatic regarding the electronic subsystem due to direct electronic wiring, e.g., vide infra), additional transfers of two protons each occurring at the distance of ca. 3 Å may provide the nonadiabaticity (see further discussion below).⁽³³⁻³⁵⁾

Evidence for the Direct Wiring of Electron Exchange through CNTs

Making the important choice between eqs 3 and 4, regarding the adequate (actually operating) equation, one has to take into account the fact of a close similarity of kinetic data and the data-processing results from the published^(12, 21, 22) and present work (Figures 1 and 2, Supporting Information Tables S4, S5). One may conclude that apparently large electron-transfer distance for GOx (with FAD moiety buried ca. 15 Å below the protein “surface”,⁽⁸⁻¹⁰⁾ compared to the case of directly adsorbed FAD, does not really matter at all, since it does not give any difference in experimentally detectable ranges for k_{ET}^0 or λ_0 . This similarity, first of all, unusually large values of k_{ET}^0 for GOx, when carbon nanotubes were exploited as the electrode extensions, has been noticed by other authors as well (see Guiseppi-Elie et al.⁽¹²⁾) and ascribed to the putative penetration of nanotubes’ (of 10 Å in diameter) free segments into the protein’s operational channel providing their direct access to the active site (“wiring”).⁽¹²⁾ According to ref 12, “It is believed that nanoscale ‘dendrites’ of CNT project outwards from the surface and act like bundled ultra-microelectrodes that allow access to the active site and permit direct electron transfer to the adsorbed enzyme”. The enrichment of GC-deposited electrode material (carbon nanotube–polymer matrix) by respective carboxylate and amine charged groups should provide excellent sliding ability for such a penetration. This conclusion seems rather realistic taking into account the published structural data⁽⁸⁻¹⁰⁾ and respective results of the computer simulation studies freely available from the Department of Chemistry, Cambridge University (2003), see: <http://www-jmg.ch.cam.ac.uk/stuff/go/go6.html>. Indeed, the “substrate channel” and its immediate neighborhood inside this protein seem to be very incompact and certainly should also be flexible enough to allow, e.g., reconstruction of its apo-form with FADs which can be beforehand tethered to Au electrodes (as in elegant experiments by Willner et al.^(13, 56) and

Gooding et al.^(14, 15, 57)). Gooding et al.⁽¹⁵⁾ also considered direct (close) contact of GOx-residing FADs with a wiring agent such as CNT, however at the cost of the substantial denaturation of GOx species, rather than the direct penetration into (almost) native protein interior; however, recent FTIR and far-UV CD studies on the conformational condition of GOx interacting with CNT-based electrodes⁽⁵⁸⁾ indicated insignificant conformational changes that may reflect only minor denaturing trend.

Interestingly, Gray et al. some time ago reported⁽⁵⁹⁾ on the direct wiring of the topaquinone (TPQ) cofactor deeply buried in *Arthrobacter globiformis* amine oxidase (AGAO) protein to Au-bead electrodes modified by the diethylaniline-terminated oligo(phenylethynyl)thiol (DEA-OPE-SH) SAMs (note at least 8 Å van der Waals diameter for the “safely penetrating” diethylaniline terminal group). Application of much thinner (“naillike”) carbon-based materials (see, e.g., ref 60), obviously, may provide potentially much less damaging methodology for direct wiring in the future. Furthermore, the narrower character of CV peaks for GOx compared to those of the isolated FAD, already discussed above, is an additional strong evidence in favor of the CNT direct penetration into the central interior part of GOx, such to provide the nearly equal possibility of ET from/to both FADs residing inside GOx (this statement does not imply that both FADs transfer electrons simultaneously, but rather behave just as statistically independent entities positioned in an almost similar position vs the CNT wire). This interaction, due to its very special character, can be assigned as nonbiological, yet specific biomimicking “recognition”. In contrary, in a reference system encompassing isolated FADs, the latter entities, due to a lack of the specific recognition motif, can be adsorbed on CNTs in much more random manner, leading to the broader spatial distribution of redox-active FAD species compared to redox-active GOx species. From the above-made conclusions, it follows automatically that the nonadiabaticity of the entire concerted process originates not from the hindrance for electronic translocations (due to direct wiring of the electrode to FAD in both cases of nanotube-tethered GOx and isolated FAD), but rather because of unavoidable tunneling pattern for the participating two protons.

Role of a Conformational Mode in Light of the Arrhenius Testing

Since the above-mentioned FAD inner-sphere reorganization unavoidably occurs in both cases of isolated FAD and GOx molecule (latter being additionally flexibilized by penetration of the nanotube moiety), similarity of respective peak shift (overvoltage) patterns (Figure 3) does not seem unexpected. Interestingly, Demin and Hall,⁽²¹⁾ using GOx that was hexahistidine-tagged at the electrode, observed even 2 orders of magnitude faster redox process compared to one at activated nanotube electrodes. It can be conjectured that in that case GOx molecules under the hexahistidine-tagged conditions preserved more nativelylike conformation compared to one with using much more bulky nanotube branches, presumably causing some conformational stress, extra flexibility, and even slight partial denaturation (vide supra). On the contrary, in the case of hexahistidine-tagged GOx, seemingly, the FAD moieties inside GOx molecules could be captured (“frozen”) in the planar configuration and would not undergo sizable inner-sphere reorganization (with a large contribution to $\Delta G_{a(\text{exp})}$, vide infra). Consequently, resulting values of respective activation Gibbs energies were lowered dramatically leading to ca. 100× increase of the operational rate constant.⁽²¹⁾

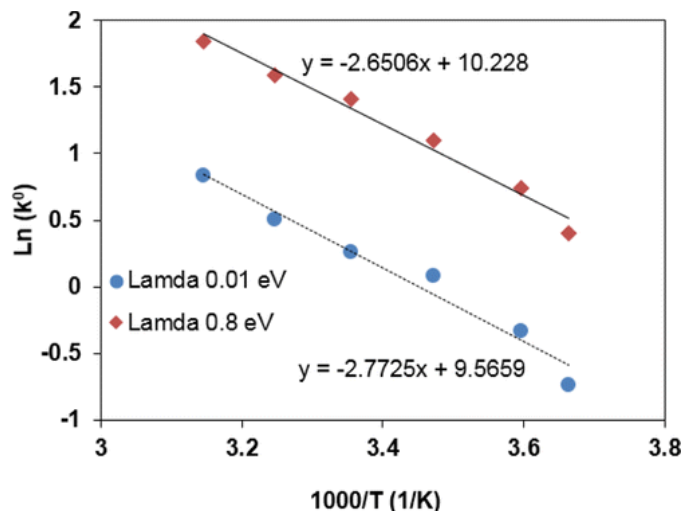


Figure 5. Arrhenius plots for $k_{\text{ET(NA)}}^0$ for two-electron exchange for a SWCNT/PEI/GOX electrode within 0–45 °C parts with selected reorganization energy. Solid lines indicate linear fittings of plots (see text). (This figure is using data from Supporting Information Table S5.)

The temperature-assisted voltammetry studies have been performed aiming to shed a light on this issue. The Arrhenius plots were composed for two sets of experimental (effective) values of $k_{\text{(eff)}}^0$ determined by using the CV data collected at lower and higher overvoltages, Figure 5. The activation enthalpy yielded nearly the same values for the both cases, $\Delta H_{\text{a(eff)}} \approx 0.24 \pm 0.01$ eV. Implying the energy wells of mostly quartic shape (Figure 4), as a simplified model for more realistic situation considered by Matyushov,^(43, 44) one can see that the results of our Arrhenius studies are in the apparent contradiction with the above-made deduction that different parts of these inharmonic wells should result in different apparent reorganization energies, hence in different effective enthalpies of activation as well. Furthermore, not only the constancy of $\Delta H_{\text{a}}^* \approx 0.24$ eV, but also its considerably large value, contradicts another experimental observation of apparently very low value of $\lambda_{\text{o(eff)}}$ deducible at low overvoltages (vide supra). On the other hand, as already mentioned above, seemingly, FAD’s specific conformational transformation, if not eliminated by the protein matrix or other biomimicking microenvironment,^(21, 61) may contribute significantly to the activation energy, hence the rate constant. Bond et al.⁽²⁰⁾ portrayed this interesting issue in terms of the “ET gating by a preceding conformational transformation”. However, traditionally, the term “gating” is more practicable in cases where the stage that precedes ET is well-separable from the elementary ET event.⁽⁵⁰⁾ Rather, we refer to the well-known instance in which some distinguished degree of freedom is involved, motion along which (that is, respective thermal activation) is a prerequisite to ET, but does not affect directly the dependence of Gibbs energy on the overpotential. Indeed, in the framework of an advanced, yet classical Marcus theory,^(29, 62) this kind of contribution has been introduced as a “work term” which can be presented as a part of experimental free energy of activation

$$\Delta G_{\text{a(exp)}} = W_i + \Delta G_{\text{a}}^* \quad (6)$$

where W_i stands for a “work term” implying the Gibbs energy of creation of a configuration in which the ET event can be realized.^(29, 62) We note again that in this model of ET, the subprocess contributing to W_i is an inseparable part of the overall (proton-coupled) ET event. For simplicity, we also assume that $W_i \approx W_{\text{f}}$, that is, the work terms for the forward and reverse ET events are

virtually identical. We also have to assume that the value of W_i , seemingly, mostly has the enthalpic nature, essentially constituting the experimental value of $\Delta H_{a(\text{exp})} \approx 0.24$ eV, whereas the value of ΔG_a^* should mostly have the entropic nature at both low and large overpotential conditions, warranting constancy of $\Delta H_{a(\text{exp})} \approx 0.24 \pm 0.01$ eV at both the low and high effective values (0.01–0.8 eV) of effective $\lambda_{0(\text{eff})}$. Large entropic contribution to the inner-sphere reorganization of the protein-assisted ET was reported earlier in the theoretical work by Cascella et al.⁽⁶³⁾ Furthermore, one has to ascribe the potential-dependent part of the activation process, ΔG_a^* (implying its prevalingly entropic underpinning), mostly to the inner-sphere reorganization of the FAD moiety heavily solvated by the water clusters. Such an attribution seems to be another necessary prerequisite for the proper understanding of above-discussed kinetic and mechanistic similarities for the GOx-encapsulated and “naked” FADs.

Numerical Estimations for the Pre-Exponential Factor

Let us now estimate the pre-exponential factor of eq 3, according to the general, here accepted quasi-simultaneous proton-coupled two-electron transfer (exchange) model. As mentioned above, $V_{AB} = H^{(\text{eff})}_{AB} \times L_{AB}$, where for the value of $H^{(\text{eff})}_{AB}$, for the case of a quasi-simultaneous two-electron transfer, according to eq 23 of ref 64, the following holds:

$$H^{(\text{eff})}_{AB} = H^{(2)}_{AB} \approx [H^{(1)}_{AB}]^2 / \lambda_0 \quad (7)$$

Here $H^{(1)}_{AB}$ indicates the electronic coupling for one-electron transfer process, whereas $H^{(2)}_{AB}$ is for two-electron transfer event occurring under otherwise similar conditions (should not be confused with just the square of H_{AB} ; thus, $[H^{(1)}_{AB}]^2$ is a square of $H^{(1)}_{AB}$). Assuming now that $H^{(1)}_{AB} \sim 0.1$ eV—a reasonable value taking into account the almost direct contact of FAD with a nanotube terminal segment (which, however, requires further adjustment through the rigorous conformational analysis/modeling), from eq 7 one obtains $H^{(\text{eff})}_{AB} \sim 0.1$ eV (since the operational value of $\lambda_{0(\text{eff})}$ seems to be of the order of 0.1 eV, or less, vide supra). For another tunneling parameter, the overlap of protons' wave functions, one may deduce that $L^{(1)}_{AB} \sim 0.01 \div 0.05$ (dimensionless parameter); hence $L_{AB} = L^{(2)}_{AB} = L^{(\text{eff})}_{AB} \sim 10^{-4}$ to 2.5×10^{-3} ,⁽³³⁻³⁵⁾ therefore, for the resulting total electron/proton tunneling factor, one obtains $V_{AB} \sim 5 \times 10^{-5}$ eV. As a result, by using $\rho_m \approx 0.28$ eV⁻¹,⁽⁶⁵⁾ and the operational value of $\Delta G_{a(\text{exp})} \approx 0.25$ eV, one can finally achieve the operational value of the standard rate constant, about the order of $k^0_{\text{ET(NA)}} \approx 2 \pm 1$ s⁻¹ (at 25 °C), in overall confirming the nonadiabatic mechanism with quasi-simultaneous two-electron transfer coupled to the rate-determining translocations of two protons. In this context, the dynamically controlled (apparently adiabatic) mechanism, eq 4, can be excluded, taking into account at least two reasons: (a) observation of hydrogen kinetic isotope effects for the GOx reaction (although not for this particular one) indirectly points to the involvement of at least one proton in the kinetic stage,^(1-7, 32-35) and (b) if eq 4 is operative, the parameter v_{eff} cannot be virtually the same for the FAD redox process occurring inside two absolutely different environments: the CNT/aqueous electrolyte junction and the GOx interior.

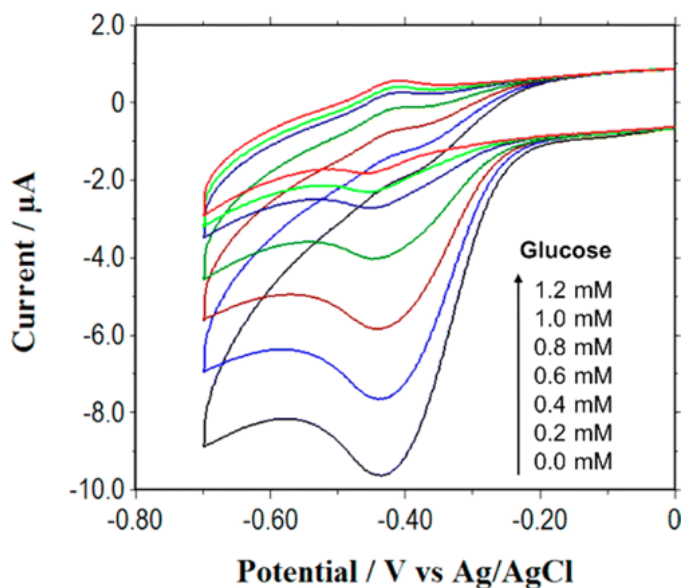
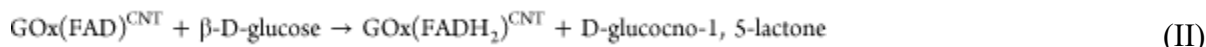


Figure 6. Representative CVs (at scan rate 50 mV/s) of GOx entrapped in CNT/PEI matrix in air-equilibrated PBS solution by adding the glucose in the solution.

The Electrocatalytic Effect of Glucose Confirming the Intact Structure of the Entrapped GOx

Recently some researchers reported^(16, 19) that when GOx is attached to the CNT matrix, it turns inactive against its substrate, glucose, in the presence of oxygen as a mediator. In general, the electrochemical pattern of GOx may involve the following reactions:



In those studies,^(16, 19) obviously, the electrocatalytic oxidation of glucose by GOx (reactions I and II) did not occur, indicating that GOx entities entrapped by CNTs were not enzymatically active. The electrochemical signal attributable to electron exchange (reaction III) was ascribed to FAD entities residing at CNTs outside GOx species, as a result of an essential GOx denaturation.

In contrast to the above-mentioned studies,^(16, 19) in this work, exploring GOx entities brought in contact with the PEI-modified CNTs, we observed the high enzymatic activity of GOx suggesting direct wiring to the CNT/PEI system, along with the essential intactness (operational validity) of GOx as an enzyme. Figure 6 shows CVs of the GOx/CNT/PEI/GC electrode while adding up to 1.2 mM glucose into the respective air-equilibrated solution (to be compared, e.g., to Figure 3B of ref 16). Initially (no glucose added), one can see the CV signal due to the reduction of O₂ (reaction I) overlapped with one attributable to the two-electron exchange of GOx(FAD) with the CNT/PEI/GC electrode (reaction III), with a redox potential at ca. -0.45 V

(vs Ag/AgCl). Upon adding glucose, a significant decrease of a cathodic peak observable at ca. -0.45 V, accompanied by the simultaneous increase of the anodic peak, is noticeable (see also Figures S12, S13 in the Supporting Information for the control tests). Finally, at the saturating concentration of glucose, reactions I and II are mutually eliminated, and what remains is the CV response due to the above-considered two-electron exchange process (reaction III). This is because the reaction I produces GOx(FAD) and reaction II produces GOx(FADH₂). Within the Supporting Information, one finds additional CV data representing the necessary control experiments. In conclusion, our results provide clear and unequivocal evidence for the essential electroactivity and direct participation of the wired GOx in the enzymatic oxidation of glucose during the mediator-free electron-transfer reaction of FAD natively embedded into a GOx protein globule.

4 Conclusions

In summary, our comparative analysis of kinetic data and respective results of the Marcus theory-based treatment for immobilized FAD and GOx essentially supports the former conjecture by Guiseppi-Elie et al.⁽¹²⁾ and the followers⁽¹³⁻¹⁵⁾ that FADs inside GOx are directly wired to the GC electrode; presumably, via close contact of nanotubes that deeply penetrate the GOx's "substrate channel", with FADs residing inside the GOx biomolecules. Importantly, this deduction is much better corroborated in this work, since the CV peak shape analysis (Figure 1 and the Supporting Information) for GOx and "naked" FAD obviously indicates much more homogeneous configurational distribution of redox-active GOx species compared to the one for naked FADs, indicating that the CNT free tail component, acting as a nanoelectrode, approaches two FADs residing inside GOx's, presumably, in an almost symmetrical configuration (keeping both FADs in a nearly indistinguishable position with regard to the ET event, *vide supra*). Moreover, we founded our introductory mechanistic analysis on the data-fitting algorithm which is based on the Marcus theory, hence taking into the account the curved character (parabolic shape) of the resultant Gibbs energy wells determining the ET event. Although our further careful analysis indicated that the actual shape of these energy wells is even more complicated (seemingly containing a large higher-order contribution), we rejected Laviron's approach⁽⁶⁶⁾ which is based on the Butler–Volmer theory using solely linear approximations for energy wells; see the Supporting Information and ref 23 (pp 97–98, 250) and ref 67.

Furthermore, the extended mechanistic analysis based on the generalized charge-transfer theory for the proton-coupled electron transfer,⁽³²⁻³⁴⁾ furnished by the first-time temperature-allied extension of protein film voltammetry, essentially supports recent deduction by Bond et al.⁽²⁰⁾ in favor of a quasi-simultaneous two-electron transfer mechanism (Note, both, the "true" simultaneous and quasi-simultaneous two-electron transfer mechanisms, according to basic physicochemical notions, should display very similar CV patterns shown in Figure 1; the quasi-simultaneous mechanism has been deduced based on the well-recognizable condition, *viz.*, the existence of an intrinsic thermodynamic asymmetry between two electrons to be transferred, *vide supra*; see also ref 20). In addition, the "anomalies" disclosed through the simulation procedure suggest deviations from the "classical" Marcus' model that implied the medium's linear response. This deduction directly follows from the shape of the peak shift versus scan rate curves depicted in Figure 3, which obviously does not match the parabolic shape for the Gibbs energy wells (linked to the medium's linear response); note this kind of anomaly has been shown to be

the common occurrence for slowly relaxing glass-forming environments such as protein interiors, organic polymers, or viscous liquids,^(43, 44) (see also ref 45).

Our careful cross-testing analysis in addition suggests that the overall two-electron transfer mechanism also is of nonadiabatic nature, controlled by the hindered (tunneling) translocations of protons rather than properly wired electrons, since, as mentioned above, the quasi-simultaneous two-electron transfer is greatly facilitated by the deep penetration and close approach of polymer-modified CNTs to FAD entities residing inside GOx interiors. Note, under the concerted proton-coupled two-electron transfer conditions, the actual proton-translocation distances (ca. 3 Å for each) occur around the FAD core (either naked or buried inside GOx), and according to the contemporary theoretical notions, the tunneling is unavoidable, eventually causing nonadiabaticity⁽³³⁻³⁵⁾ (despite a wiring pattern for the transferred electrons, hence their adiabatic participation in the overall concerted process). The accompanying inner-sphere conformational transformation of FAD then may contribute the rate constant through the strong prearrangement process and thermally activated work-term input (being the inseparable parts of the overall concerted process), however, not through the “gating” pattern, as conjectured before. As discussed in the respective subsection above, the mentioned conformational transformation of FAD (hence its large input into the overall Gibbs energy pattern) can be probably eliminated under more natively like conditions for GOx (e.g., by applying of a much less perturbative wiring tool compared to ours), when the protein matrix remains rather inflexible (“frozen”) and does not allow strongly confined FAD cofactors to create the extra thermally activated contribution.^(20, 21, 61)

Finally we note that, although a multitude of the mechanistic aspects discussed in this paper point to the extreme complexity of an entire pattern of the studied process, all these aspects are intrinsically and inseparably connected in an essentially synergic way; that is, each of the deductions rests on a variety of others and, in turn, supports them, thus, overall forming a tentative, yet promising account. Therefore, it seems realistic that the ultimate model of the future, exhaustively describing the whole GOx machinery, would entail the key narrative elements of this work.

Supporting Information

Additional experiment, data analysis and discussions, supporting figures and tables. The Supporting Information is available free of charge on the ACS Publications website at DOI: 10.1021/acs.jpcc.5b02796.

Acknowledgment

J.W. acknowledges the support from JSNN; J.W. and S.S. also acknowledge the partial financial support from the DOD SBIR/STTR program; T.D.D. and D.E.K. kindly acknowledge the financial support from the Rustaveli National Science Foundation (Georgian Republic).

References

1. Wilson, R.; Turner, A. P. F. Glucose Oxidase: An Ideal Enzyme Biosens. *Bioelectron.* **1992**, *7*, 165– 185
2. Leskovac, V.; Trivić, S.; Wohlfahrt, G.; Kandrač, J.; Peričin, D. Glucose Oxidase from *Aspergillus Niger*: The Mechanism of Action with Molecular Oxygen, Quinones, and One-Electron Acceptors *Int. J. Biochem. Cell Biol.* **2005**, *37*, 731– 750
3. Heller, A.; Feldman, B. Electrochemical Glucose Sensors and Their Applications in Diabetes Management *Chem. Rev.* **2008**, *108*, 2482– 2505
4. Su, Q.; Klinman, J. P. Nature of Oxygen Activation in Glucose Oxidase from *Aspergillus Niger*: The Importance of Electrostatic Stabilization in Superoxide Formation *Biochemistry* **1999**, *38*, 8572– 8581
5. Roth, J. P.; Klinman, J. P. Catalysis of Electron Transfer during Activation of O₂ by the Flavoprotein Glucose Oxidase *Proc. Natl. Acad. Sci. U.S.A.* **2003**, *100*, 62– 67
6. Roth, J. P.; Wincek, R.; Nodet, G.; Edmondson, D. E.; McIntire, W. S.; Klinman, J. P. Oxygen Isotope Effects on Electron Transfer to O₂ Probed Using Chemically Modified Flavins Bound to Glucose Oxidase *J. Am. Chem. Soc.* **2004**, *126*, 15120– 15131
7. Brinkley, D. W.; Roth, J. P. Determination of a Large Reorganization Energy Barrier for Hydride Abstraction by Glucose Oxidase *J. Am. Chem. Soc.* **2005**, *127*, 15720– 15721
8. Hecht, H. J.; Kalisz, H. M.; Hendle, J.; Schmid, R. D.; Schomburg, D. Crystal Structure of Glucose Oxidase from *Aspergillus Niger* Refined at 2.3 Å Reslution *J. Mol. Biol.* **1993**, *229*, 153– 172
9. Hecht, H. J.; Schomburg, D.; Kalisz, H.; Schmid, R. D. The 3D Structure of Glucose Oxidase from *Aspergillus Niger*. Implications for the Use of GOD as a Biosensor Enzyme Biosens. *Bioelectron.* **1993**, *8*, 197– 203
10. Wohlfahrt, G.; Witt, S.; Hendle, J.; Schomburg, D.; Kalisz, H. M.; Hecht, H.-J. 1.8 and 1.9 Å Resolution Structures of the *Penicillium Amagasakiense* and *Aspergillus Niger* Glucose Oxidases as a Basis for Modelling Substrate Complexes *Acta Crystallogr., Sect. D: Biol. Crystallogr.* **1999**, *55*, 969– 977
11. Mano, N.; Mao, F.; Heller, A. A Miniature Membrane-Less Biofuel Cell Operating at +0.60 V under Physiological Conditions *ChemBioChem* **2004**, *5*, 1703– 1705
12. Guiseppi-Elie, A.; Lei, C.; Baughman, R. H. Direct Electron Transfer of Glucose Oxidase on Carbon Nanotubes *Nanotechnology* **2002**, *13*, 559
13. Patolsky, F.; Weizmann, Y.; Willner, I. Long-Range Electrical Contacting of Redox Enzymes by SWCNT Connectors *Angew. Chem., Int. Ed.* **2004**, *43*, 2113– 2117

- 14.** Liu, J.; Chou, A.; Rahmat, W.; Paddon-Row, M. N.; Gooding, J. J. Achieving Direct Electrical Connection to Glucose Oxidase Using Aligned Single Walled Carbon Nanotube Arrays *Electroanalysis* **2005**, *17*, 38– 46
- 15.** Liu, J.; Paddon-Row, M. N.; Gooding, J. J. Heterogeneous Electron-Transfer Kinetics for Flavin Adenine Dinucleotide and Ferrocene through Alkanethiol Mixed Monolayers on Gold Electrodes *J. Phys. Chem. B* **2004**, *108*, 8460– 8466
- 16.** Wooten, M.; Karra, S.; Zhang, M.; Gorski, W. On the Direct Electron Transfer, Sensing, and Enzyme Activity in the Glucose Oxidase/Carbon Nanotubes System *Anal. Chem.* **2014**, *86*, 752– 757
- 17.** Smith, E. T.; Davis, C. A.; Barber, M. J. Voltammetric Simulations of Multiple Electron Transfer/Proton Transfer Coupled Reactions: Flavin Adenine Dinucleotide as a Model System *Anal. Biochem.* **2003**, *323*, 114– 121
- 18.** Cable, M.; Smith, E. T. Identifying the N = 2 Reaction Mechanism of FAD through Voltammetric Simulations *Anal. Chim. Acta* **2005**, *537*, 299– 306
- 19.** Goran, J. M.; Mantilla, S. M.; Stevenson, K. J. Influence of Surface Adsorption on the Interfacial Electron Transfer of Flavin Adenine Dinucleotide and Glucose Oxidase at Carbon Nanotube and Nitrogen-Doped Carbon Nanotube Electrodes *Anal. Chem.* **2013**, *85*, 1571– 1581
- 20.** Simonov, A. N.; Grosse, W.; Mashkina, E. A.; Bethwaite, B.; Tan, J.; Abramson, D.; Wallace, G. G.; Moulton, S. E.; Bond, A. M. New Insights into the Analysis of the Electrode Kinetics of Flavin Adenine Dinucleotide Redox Center of Glucose Oxidase Immobilized on Carbon Electrodes *Langmuir* **2014**, *30*, 3264– 3273
- 21.** Demin, S.; Hall, E. A. H. Breaking the Barrier to Fast Electron Transfer *Bioelectrochemistry* **2009**, *76*, 19– 27
- 22.** Sheng, Q.; Luo, K.; Li, L.; Zheng, J. Direct Electrochemistry of Glucose Oxidase Immobilized on NdPO₄ Nanoparticles/Chitosan Composite Film on Glassy Carbon Electrodes and Its Biosensing Application *Bioelectrochemistry* **2009**, *74*, 246– 253
- 23.** Bard, A. J.; Faulkner, L. R. *Electrochemical Methods: Fundamentals and Applications*, 2nd ed.; John Wiley: New York, 2001.
- 24.** Polcyn, D. S.; Shain, I. Multistep Charge Transfers in Stationary Electrode Polarography *Anal. Chem.* **1966**, *38*, 370– 375
- 25.** Voet, J. G.; Coe, J.; Epstein, J.; Matossian, V.; Shipley, T. Electrostatic Control of Enzyme Reactions: Effect of Ionic Strength on the pK_a of an Essential Acidic Group on Glucose Oxidase *Biochemistry* **1981**, *20*, 7182– 7185

- 26.** Wei, J. J.; Liu, H.; Niki, K.; Margoliash, E.; Waldeck, D. H. Probing Electron Tunneling Pathways: Electrochemical Study of Rat Heart Cytochrome *C* and Its Mutant on Pyridine-Terminated Sams J. Phys. Chem. B **2004**, 108, 16912– 16917
- 27.** Marcus, R. A. On the Theory of Electron-Transfer Reactions. VI. Unified Treatment for Homogeneous and Electrode Reactions J. Chem. Phys. **1965**, 43, 679– 701
- 28.** Dogonadze, R. R.; Kuznetsov, A. M. Theory of Charge Transfer Kinetics at Solid–Polar Liquid Interfaces Prog. Surf. Sci. **1975**, 6, 1– 41
- 29.** Marcus, R. A.; Sutin, N. Electron Transfers in Chemistry and Biology Biochim. Biophys. Acta, Bioenerg. **1985**, 811, 265– 322
- 30.** Zusman, L. D. Dynamic Solvent Effects in Electron Transfer Reactions Z. Phys. Chem. (Munche) **1994**, 186, 1– 29
- 31.** Bixon, M.; Jortner, J., Electron Transfer—From Isolated Molecules to Biomolecules. In Advances in Chemical Physics; John Wiley & Sons, Inc.: New York, 2007; pp 35– 202.
- 32.** Migliore, A.; Polizzi, N. F.; Therien, M. J.; Beratan, D. N. Biochemistry and Theory of Proton-Coupled Electron Transfer Chem. Rev. **2014**, 114, 3381– 3465
- 33.** Kuznetsov, A. M.; Ulstrup, J. Dynamics of Low-Barrier Proton Transfer in Polar Solvents and Protein Media Chem. Phys. **1994**, 188, 131– 141
- 34.** Krishtalik, L. I. The Mechanism of the Proton Transfer: An Outline Biochim. Biophys. Acta, Bioenerg. **2000**, 1458, 6– 27
- 35.** Shushanyan, M.; Khoshtariya, D. E.; Tretyakova, T.; Makharadze, M.; van Eldik, R. Diverse Role of Conformational Dynamics in Carboxypeptidase a-Driven Peptide and Ester Hydrolyses: Disclosing the “Perfect Induced Fit” and “Protein Local Unfolding” Pathways by Altering Protein Stability Biopolymers **2011**, 95, 852– 870
- 36.** Weber, K.; Creager, S. E. Voltammetry of Redox-Active Groups Irreversibly Adsorbed onto Electrodes. Treatment Using the Marcus Relation between Rate and Overpotential Anal. Chem. **1994**, 66, 3164– 3172
- 37.** Weber, K.; Hockett, L.; Creager, S. Long-Range Electronic Coupling between Ferrocene and Gold in Alkanethiolate-Based Monolayers on Electrodes J. Phys. Chem. B **1997**, 101, 8286– 8291
- 38.** Tender, L.; Carter, M. T.; Murray, R. W. Cyclic Voltammetric Analysis of Ferrocene Alkanethiol Monolayer Electrode Kinetics Based on Marcus Theory Anal. Chem. **1994**, 66, 3173– 3181

- 39.** Napper, A. M.; Liu, H.; Waldeck, D. H. The Nature of Electronic Coupling between Ferrocene and Gold through Alkanethiolate Monolayers on Electrodes: The Importance of Chain Composition, Interchain Coupling, and Quantum Interference *J. Phys. Chem. B* **2001**, 105, 7699– 7707
- 40.** Miyashita, O.; Onuchic, J. N.; Wolynes, P. G. Nonlinear Elasticity, Proteinquakes, and the Energy Landscapes of Functional Transitions in Proteins *Proc. Natl. Acad. Sci. U.S.A.* **2003**, 100, 12570– 12575
- 41.** Hegler, J. A.; Weinkam, P.; Wolynes, P. G. The Spectrum of Biomolecular States and Motions *HFSP J.* **2008**, 2, 307– 313
- 42.** Meinhold, L.; Smith, J. C.; Kitao, A.; Zewail, A. H. Picosecond Fluctuating Protein Energy Landscape Mapped by Pressure–Temperature Molecular Dynamics Simulation *Proc. Natl. Acad. Sci. U.S.A.* **2007**, 104, 17261– 17265
- 43.** LeBard, D. N.; Matyushov, D. V. Glassy Protein Dynamics and Gigantic Solvent Reorganization Energy of Plastocyanin *J. Phys. Chem. B* **2008**, 112, 5218– 5227
- 44.** Matyushov, D. V. Nanosecond Stokes Shift Dynamics, Dynamical Transition, and Gigantic Reorganization Energy of Hydrated Heme Proteins *J. Phys. Chem. B* **2011**, 115, 10715– 10724
- 45.** Khoshtariya, D. E.; Dolidze, T. D.; Tretyakova, T.; van Eldik, R. Electron Transfer with Copper Ions Self-Assembled at Au-Deposited Biomimetic Films: Mechanistic “Anomalies” Disclosed by Temperature- and Pressure-Assisted Fast-Scan Voltammetry *J. Phys. D: Appl. Phys.* **2015**, 48, 255402 (11p)
- 46.** Khoshtariya, D. E.; Dolidze, T. D.; Tretyakova, T.; Waldeck, D. H.; van Eldik, R. Electron Transfer with Azurin at Au-SAM Junctions in Contact with a Protic Ionic Melt: Impact of Glassy Dynamics *Phys. Chem. Chem. Phys.* **2013**, 15, 16515– 16526
- 47.** Lakshmanan, M.; Karlsson, F.; Fröman, P. O. Phase-Integral Calculation of the Energy Levels of a Quantal Anharmonic Oscillator *Phys. Rev. D* **1981**, 24, 2586– 2598
- 48.** Yuste, S. B.; Sánchez, A. M. Energy Levels of the Quartic Double Well Using a Phase-Integral Method *Phys. Rev. A* **1993**, 48, 3478– 3485
- 49.** Wei, J.; Liu, H.; Khoshtariya, D. E.; Yamamoto, H.; Dick, A.; Waldeck, D. H. Electron-Transfer Dynamics of Cytochrome *C*: A Change in the Reaction Mechanism with Distance *Angew. Chem., Int. Ed.* **2002**, 41, 4700– 4703
- 50.** Khoshtariya, D. E.; Wei, J.; Liu, H.; Yue, H.; Waldeck, D. H. Charge-Transfer Mechanism for Cytochrome *C* Adsorbed on Nanometer Thick Films. Distinguishing Frictional Control from Conformational Gating *J. Am. Chem. Soc.* **2003**, 125, 7704– 7714

- 51.** Khoshtariya, D. E.; Dolidze, T. D.; Sarauli, D.; van Eldik, R. High-Pressure Probing of a Changeover in the Charge-Transfer Mechanism for Intact Cytochrome *C* at Gold/Self-Assembled Monolayer Junctions *Angew. Chem., Int. Ed.* **2006**, *45*, 277– 281
- 52.** Khoshtariya, D. E.; Dolidze, T. D.; Seifert, S.; Sarauli, D.; Lee, G.; van Eldik, R. Kinetic, Thermodynamic, and Mechanistic Patterns for Free (Unbound) Cytochrome *C* at Au/SAM Junctions: Impact of Electronic Coupling, Hydrostatic Pressure, and Stabilizing/Denaturing Additives *Chem.—Eur. J.* **2006**, *12*, 7007– 7007
- 53.** Khoshtariya, D. E.; Dolidze, T. D.; Shushanyan, M.; Davis, K. L.; Waldeck, D. H.; van Eldik, R. Fundamental Signatures of Short- and Long-Range Electron Transfer for the Blue Copper Protein Azurin at Au/SAM Junctions *Proc. Natl. Acad. Sci. U.S.A.* **2010**, *107*, 2757– 2762
- 54.** Dolidze, T. D.; Rondinini, S.; Vertova, A.; Waldeck, D. H.; Khoshtariya, D. E. Impact of Self-Assembly Composition on the Alternate Interfacial Electron Transfer for Electrostatically Immobilized Cytochrome *C*. *Biopolymers* **2007**, *87*, 68– 73
- 55.** Khoshtariya, D. E.; Dolidze, T. D.; Shushanyan, M.; van Eldik, R. Long-Range Electron Transfer with Myoglobin Immobilized at Au/Mixed-SAM Junctions: Mechanistic Impact of the Strong Protein Confinement *J. Phys. Chem. B* **2014**, *118*, 692– 706
- 56.** Riklin, A.; Katz, E.; Willner, I.; Stocker, A.; Bückmann, A. F. Improving Enzyme Electrode Contacts by Redox Modification of Cofactors *Nature* **1995**, *376*, 672– 675
- 57.** Liu, G.; Paddon-Row, M. N.; Gooding, J. J. A Molecular Wire Modified Glassy Carbon Electrode for Achieving Direct Electron Transfer to Native Glucose Oxidase *Electrochem. Commun.* **2007**, *9*, 2218– 2223
- 58.** Zhao, H.-Z.; Sun, J.-J.; Song, J.; Yang, Q.-Z. Direct Electron Transfer and Conformational Change of Glucose Oxidase on Carbon Nanotube-Based Electrodes *Carbon* **2010**, *48*, 1508– 1514
- 59.** Hess, C. R.; Juda, G. A.; Dooley, D. M.; Amii, R. N.; Hill, M. G.; Winkler, J. R.; Gray, H. B. Gold Electrodes Wired for Coupling with the Deeply Buried Active Site of *Arthrobacter Globiformis* Amine Oxidase *J. Am. Chem. Soc.* **2003**, *125*, 7156– 7157
- 60.** Li, K.; Liu, B.; Zheng, J.; Sheng, Q.; Liu, R. Direct Electrochemistry of Glucose Oxidase on Nail-Like Carbon and Its Biosensing for Glucose Electroanalysis **2010**, *22*, 701– 706
- 61.** Birss, V. I.; Elzanowska, H.; Turner, R. A. The Electrochemical Behavior of Flavin Adenine Dinucleotide in Neutral Solutions *Can. J. Chem.* **1988**, *66*, 86– 96
- 62.** Marcus, R. A. Enzymatic Catalysis and Transfers in Solution. I. Theory and Computations, a Unified View *J. Chem. Phys.* **2006**, *125*, 194504

- 63.** Cascella, M.; Magistrato, A.; Tavernelli, I.; Carloni, P.; Rothlisberger, U. Role of Protein Frame and Solvent for the Redox Properties of Azurin from *Pseudomonas Aeruginosa* Proc. Natl. Acad. Sci. U.S.A. **2006**, 103, 19641– 19646
- 64.** Khoshtariya, D. E.; Dolidze, T. D.; Zusman, L. D.; Lindbergh, G.; Glaser, J. Two-Electron Transfer for $Tl(Aq)^{3+}/Tl(Aq)^+$ Revisited. Common Virtual $[Tl^{II}-Tl^{II}]^{4+}$ Intermediate for Homogeneous (Superexchange) and Electrode (Sequential) Mechanisms Inorg. Chem. **2002**, 41, 1728– 1738
- 65.** Chidsey, C. E. D. Free Energy and Temperature Dependence of Electron Transfer at the Metal–Electrolyte Interface Science **1991**, 251, 919– 922
- 66.** Laviron, E. General Expression of the Linear Potential Sweep Voltammogram in the Case of Diffusionless Electrochemical Systems J. Electroanal. Chem. **1979**, 101, 19– 28
- 67.** Pletcher, D.; Greff, R.; R, P.; Peter, L. M.; Robinson, J. Instrumental Methods in Electrochemistry; Horwood Publishing: Oxford, 2001.